Supplementary data and methods
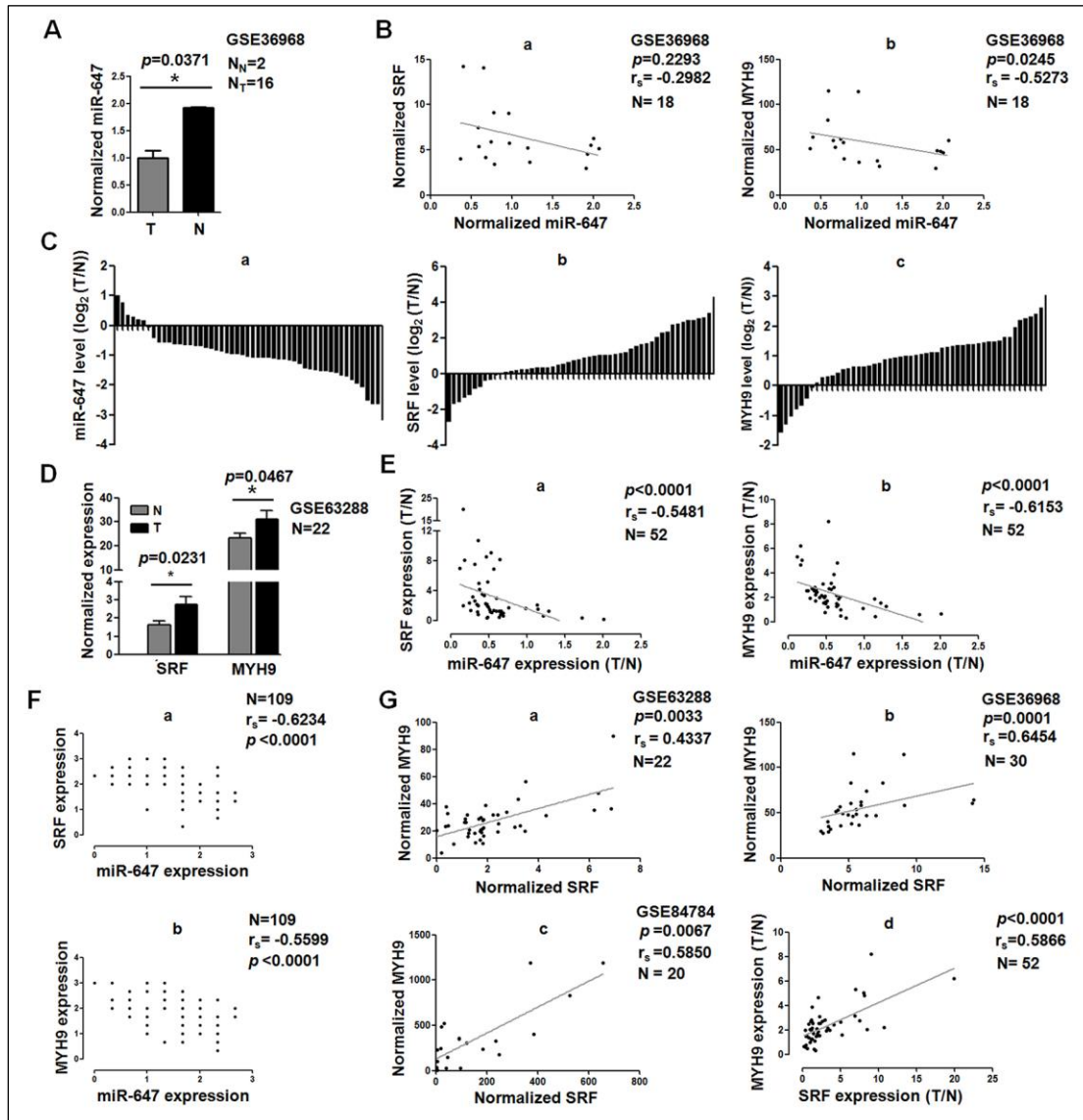
Figure S1. Analysis of miR-647, SRF and MYH9 expression in GEO database and GC patients.

(A) MiR-647 expression in GC was analyzed using data from GSE36968. (B) The correlation of miR-647 expression and SRF or MYH9 expression were analyzed using data from GSE36968. (C) The mRNA expression levels of miR-647, SRF and MYH9 were detected by qPCR in 52 pairs of GC tissues and normal gastric mucosa. (D) SRF and MYH9 expression in GC was analyzed using data from GSE63288. (E) The correlation of miR-647 expression and SRF or MYH9 expression were analyzed using qPCR data from 52 GC patients. (F) Spearman rank correlation analysis was performed to detect clinical associations of miR-647, SRF and MYH9 expression based on the ISH and IHC expression scores from 109 GC patients. (G) The correlation analysis of SRF and MYH9 expression was based on GSE63288 (a) GSE36968 (b), GSE84784(c) and qPCR data from 52 GC patients (d).
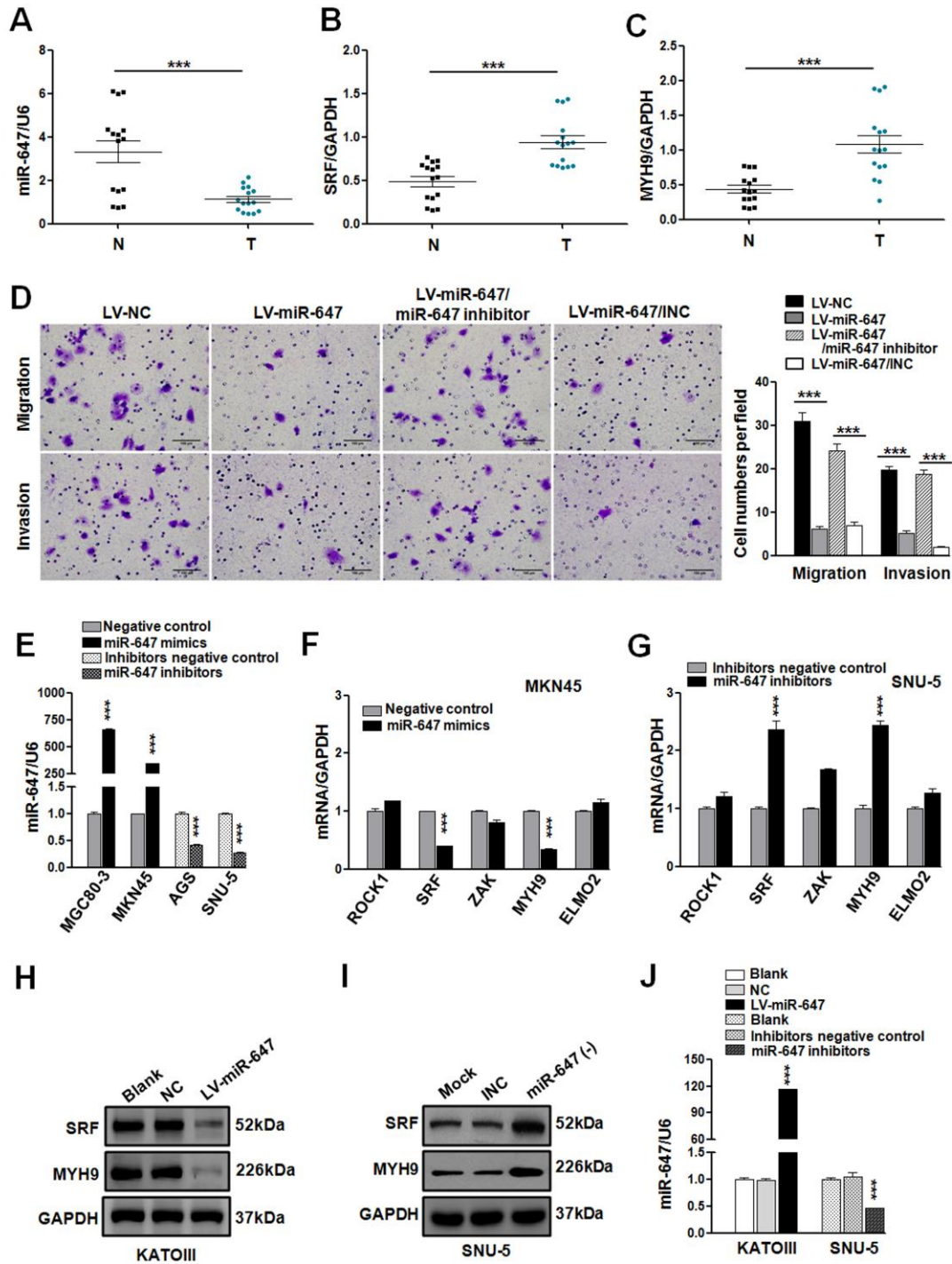
Figure S2. miR-647, which inhibited the migration and invasion of gastric cancer cell lines, was conversely associated with the expressions of SRF and MYH9.

(A-C) MiR-647, SRF and MYH9 in 5 gastric cancer cell lines compared with 5 normal gastric mucosa tissues were detected by qPCR. (D) Cell 3D migration and invasion in AGS cell lines. Cell 3D migration and invasion were tested using transwell chamber migration assay (8-µm pore size membrane) and invasion assay (Matrigel-coated membrane). AGS transfected with LV-NC, LV-miR-647, LV-miR-647 plus miR-647 inhibitor and LV-miR-647 plus INC were detected. Each bar represents the mean ± SD. The results were reproduced in three independent experiments. ***p<0.001. (E) Expression of miR-647 in gastric cancer cell lines (MGC80-3, MKN45, AGS and SNU-5) transiently transfected with miR-647 mimics or inhibitors was detected by qPCR. U6 served as an internal control. ***p<0.001. (F-G) Expression of Rho-associated genes was analyzed in MKN45 and SNU-5 was detected by qPCR. GAPDH served as an internal control. ***p<0.001. (H-J) Western blot analysis was used to detect the expression level of SRF and MYH9 in KATOIII cells (H) and SUN-5(I) after infection with miR-647 expressing or control lentivirus. GAPDH served as an internal control. (J) Expression of miR-647 in these cells transfected with LV-miR-647 or inhibitors was detected by qPCR. U6 served as an internal control. ***p<0.001.
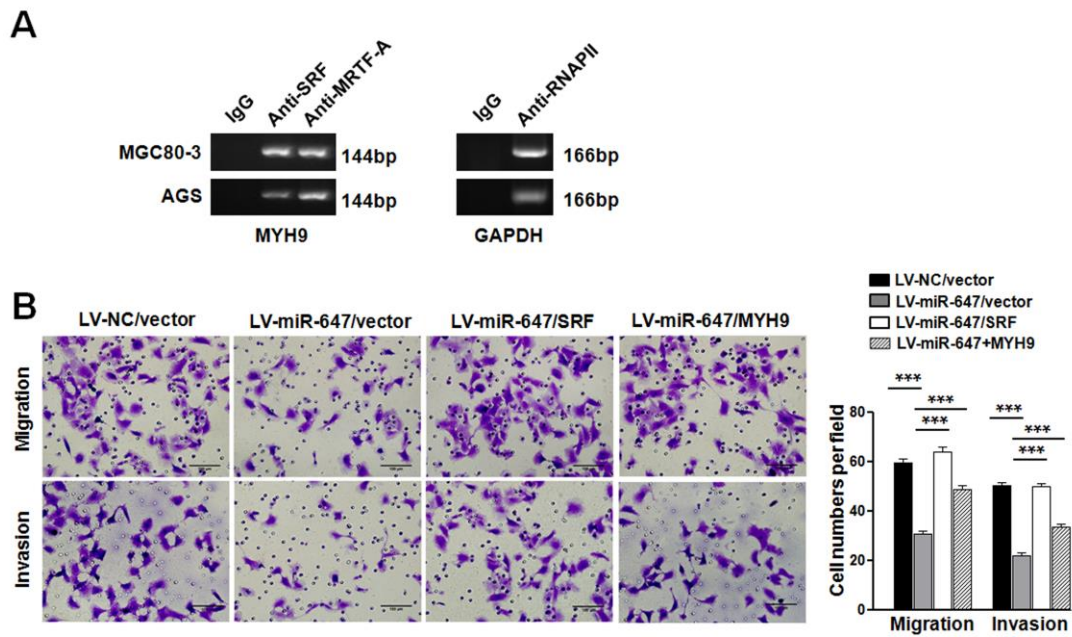
Figure S3. SRF/MYH9 axis in gastric cancer cells' migration and invasion.

(A) ChIP analysis of SRF binding to the MYH9 promoter region in MGC 80-3 and AGS cells. The image of agarose gel electrophoresis were shown. RNA polymerase II (RNAPII) antibody and GAPDH promoter primers were used as a positive control, and IgG was showed as a negative control. (B) Cell 3D migration and invasion were tested using transwell chamber migration assay and invasion assay. MGC 80-3-LV-miR-647 transfected with SRF plasmid (SRF), MYH9 plasmid (MYH9) and control vector were used. Each bar represents the mean ± SD. ***p<0.001.
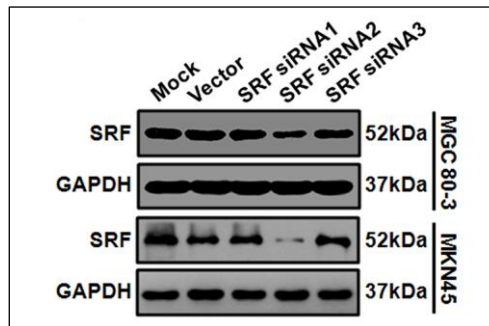
Figure S4. SRF small interfering RNA (siRNAs) specifically suppress SRF expression in GC cell lines.

The siRNAs was transfected into MGC 80-3 and MKN45, respectively. SRF and MYH9 expression were detected by western blot to choose the most effective shRNA sequence for further study.
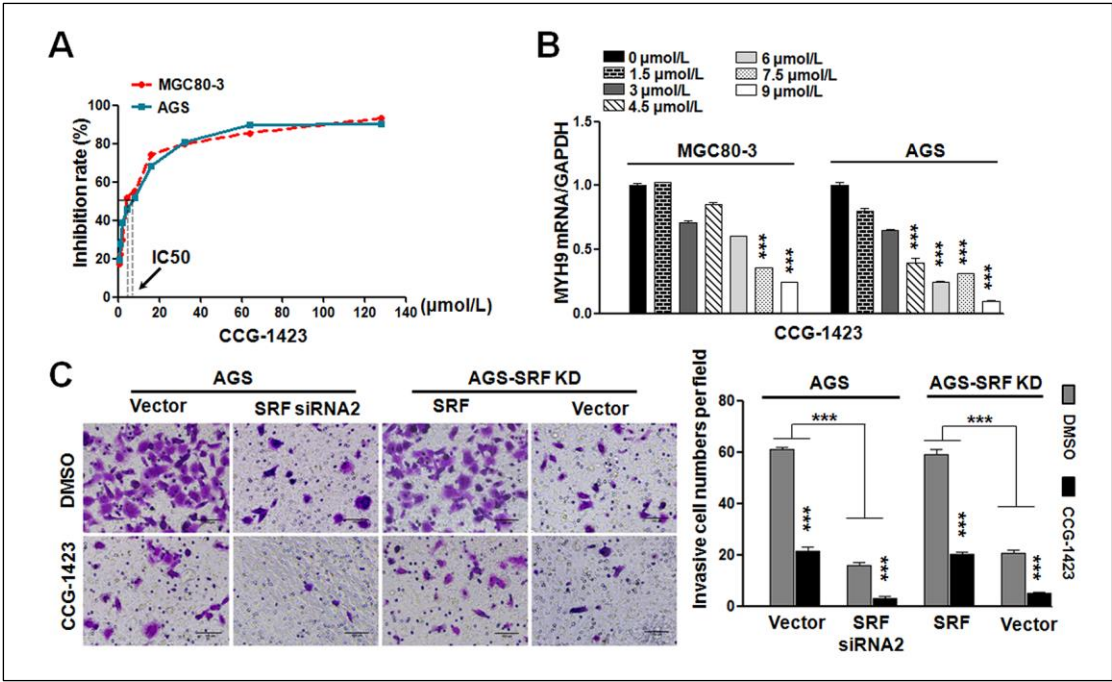
Figure S5. CCG-1423 inhibits gastric cancer cells' migration and invasion.

(A) The IC50 of CCG-1423 in MGC80-3 and AGS was detected by exposing cells in CCG-1423 with a linear concentration gradient. (B) The appropriate working concentration of CCG-1423 was determined using CCG-1423 with a linear concentration gradient.(C) Cell 3D invasion was tested using transwell chamber invasion assay (Matrigel-coated membrane). AGS transfected with SRF siRNA2 plasmid, SRF plasmid and their corresponding control vectors were detected. CCG-1423 (7.5μmol/L) and its inner control Dimethyl sulfoxide (DMSO) were used to detect their influences on gastric cancer cell invasion. ***$p<0.001$.
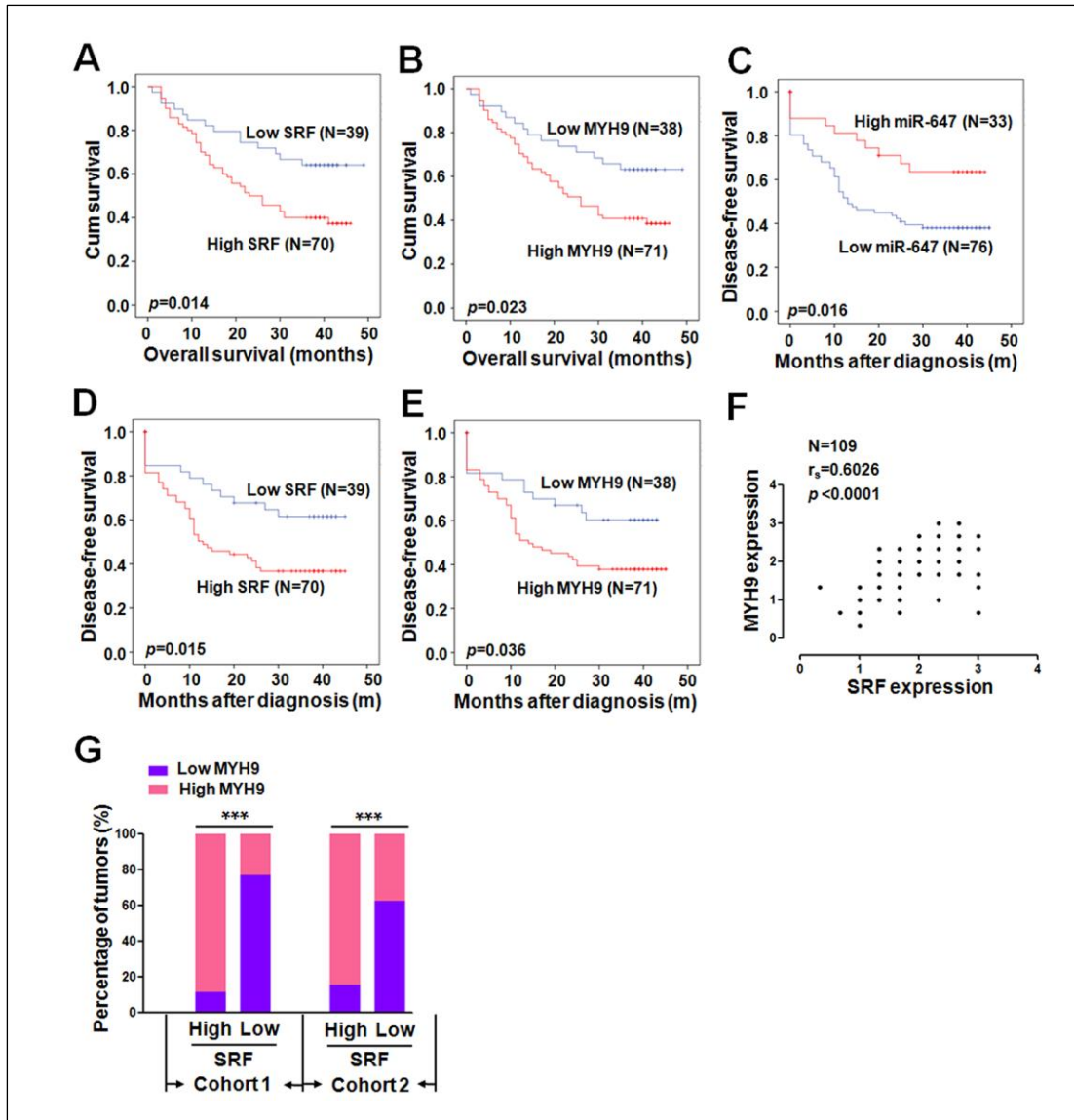
Figure S6. Clinical associations of SRF and MYH9 expression.

(A-B) Kaplan-Meier survival analysis of SRF and MYH9 expression in 109 GC patients (log-rank test) were performed to determine the correlation between their expression levels and overall survival time. (C-E) Kaplan-Meier survival analysis of miR-647, SRF and MYH9 expression in 109 GC patients (log-rank test) were performed to determine the correlation between their expression levels and disease free survival time. (F) Spearman rank correlation analysis was performed to detect clinical associations of SRF and MYH9 expression based on the IHC expression scores from 109 GC patients. (G) The percentage of specimens showing low or high SRF expression in relation to the expression levels of MYH9 in two cohorts; ***$p<0.001$.
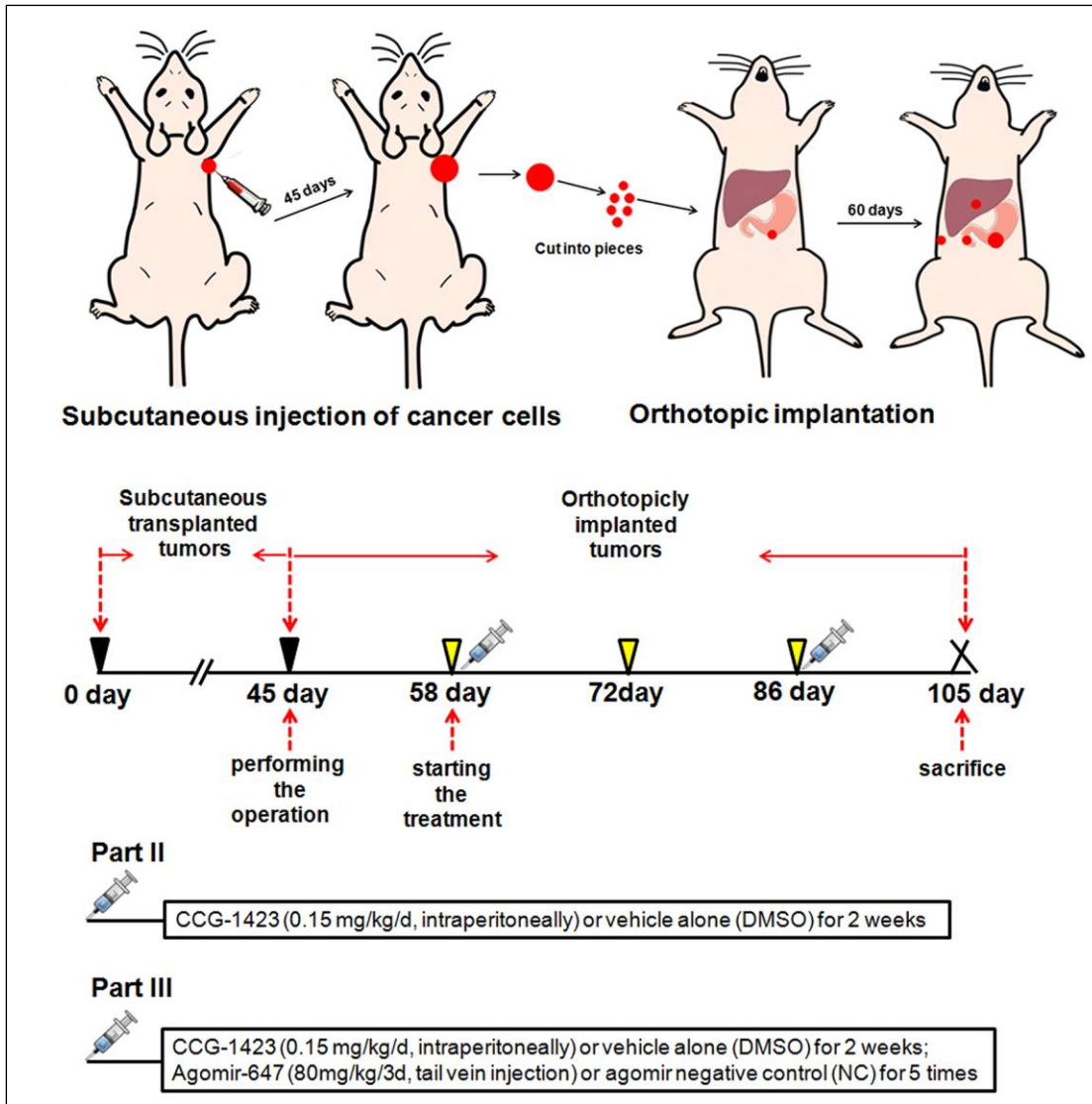
Figure S7. Illustration of human gastric cancer metastatic models and its drug administration in nude mice.

Human gastric cancer metastatic models were constructed using orthotopic implantation of cancerous tissues produced by subcutaneous injection of gastric cancer cells. CCG-1423 and agomir-647 were used to treat these metastatic orthotopic-transplant nude-mouse models.
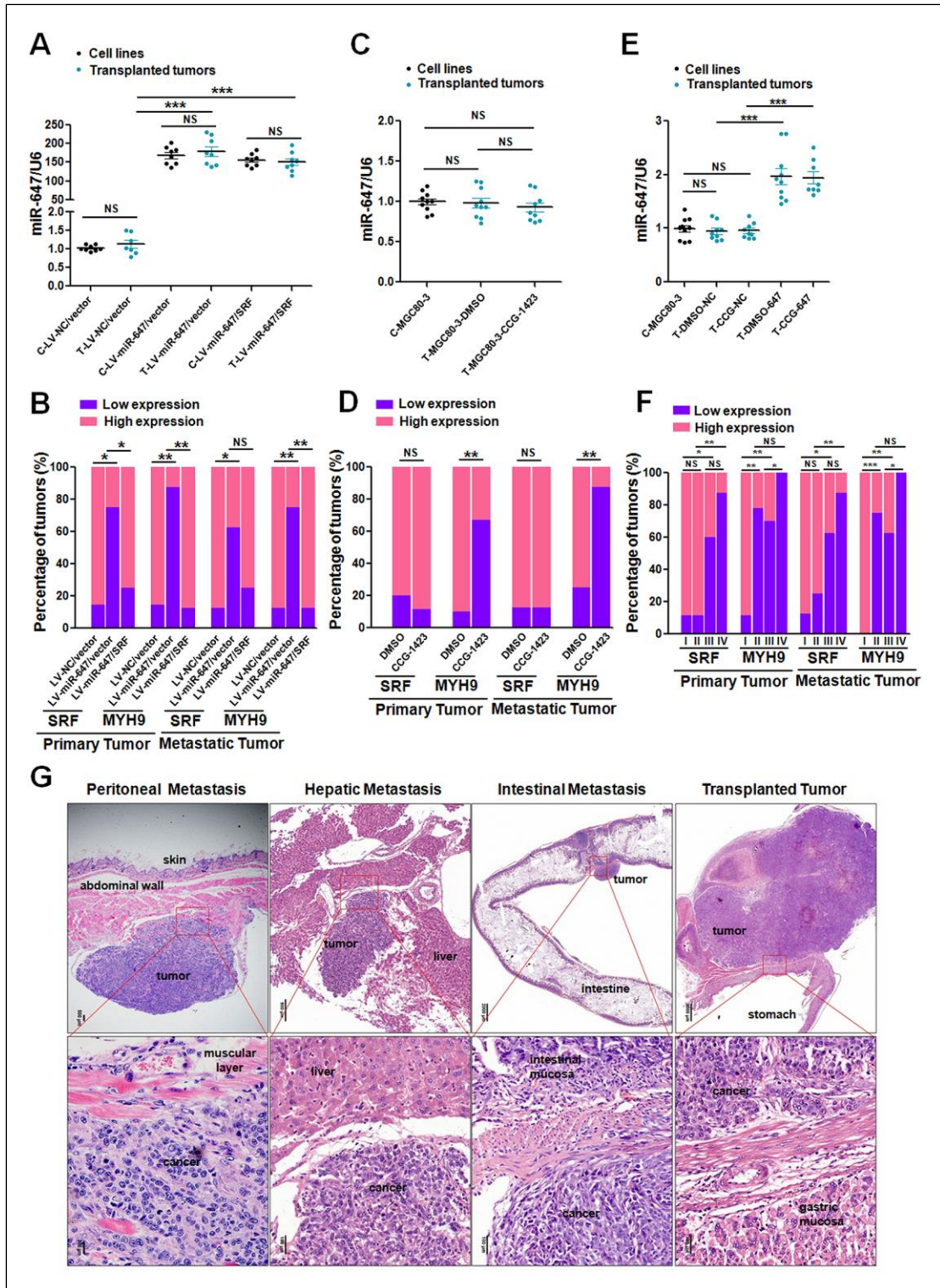
Figure S8. MiR-647, SRF and MYH9 expression in human gastric cancer metastatic models. (A-F) miR-647, SRF and MYH9 expression levels in primary tumors and the metastatic origin of these tumors were detected by qPCR and IHC. (A, C and E) miR-647 expression in MGC80-3 cells and transplanted tumors was detected by qPCR. (B, D and F) SRF and MYH9 expression levels in MGC80-3 cells and transplanted tumors were detected by IHC. The percentage of specimens showing low or high expression of SRF or MYH9 proteins in every group was shown by immunohistochemical scores; NS, no statistical significance, *p<0.05, **p<0.01, ***p<0.001. (G) Primary tumors and the metastatic nodules were detected by HE staining.
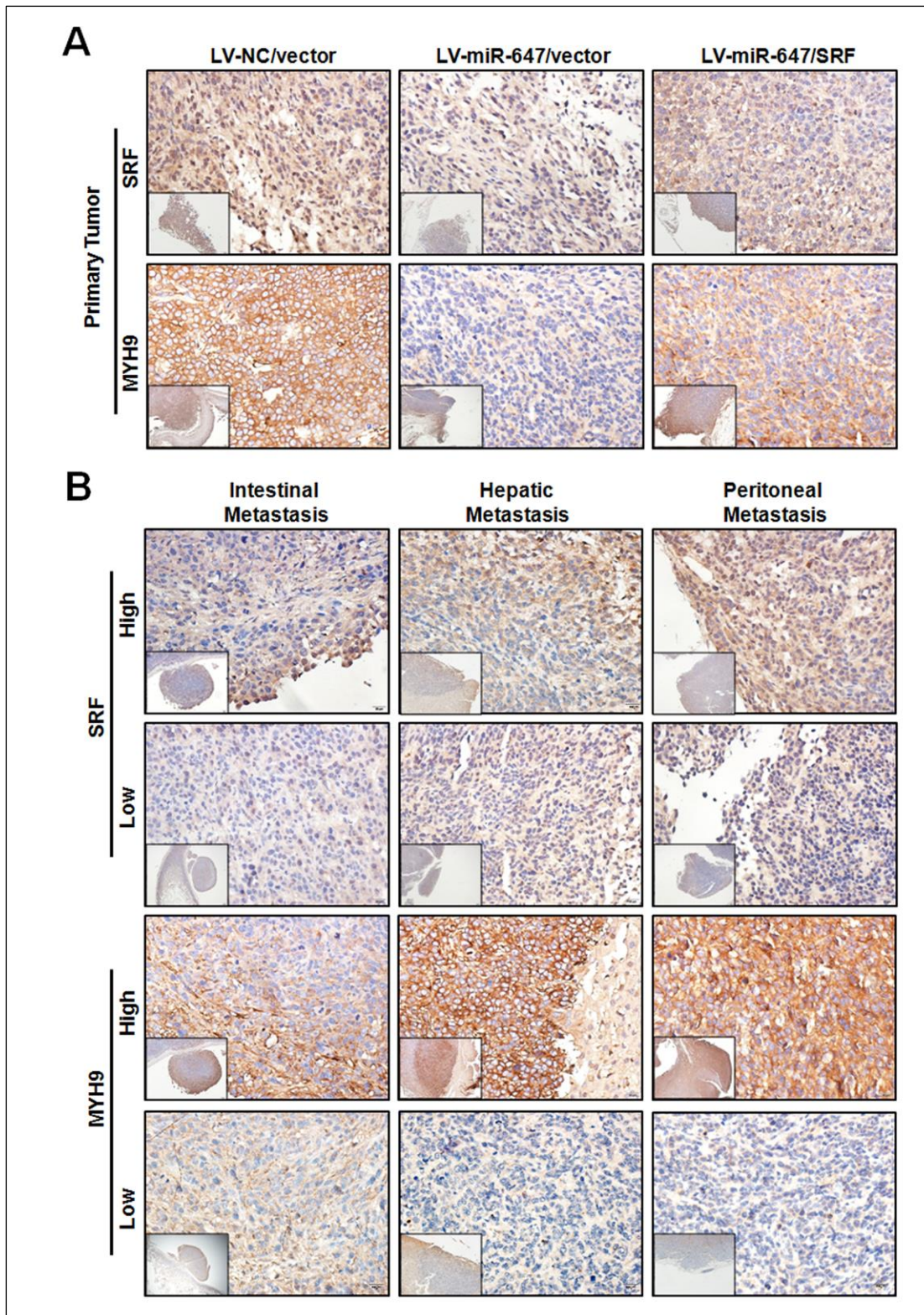
Figure S9. SRF and MYH9 expression in primary tumors and metastatic nodules.

(A) SRF and MYH9 expression levels in primary tumors of part I were detected by IHC. (B) Immunohistochemical scores based on high or low IHC staining were used to analyze the expressions of SRF and MYH9 proteins in metastatic nodules of nude mice.
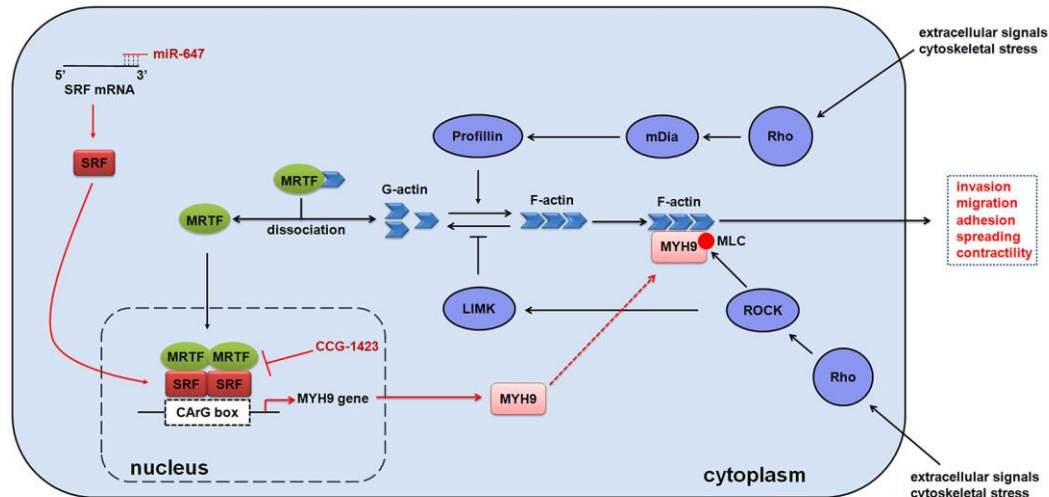
Figure S10. miR-647 and CCG-1423 inhibited gastric cancer metastasis by targeting to Rho/SRF/MYH9 pathway.
The pathway marked with black arrows refers to previous studies [1, 2]. The pathway marked with red arrows is shown in our studies.

Table S1. Clinicopathologic characteristics of GC patients

Cohort 1 (n=109)		Cohort 2 (n=90)	
Feature	**N (%)**	**Feature**	**N (%)**
Gender		**Gender**	
Male	70 (64.2)	Male	60 (66.7)
Female	39 (35.8)	Female	30 (33.3)
Median age		**Median age**	
<59 years	40 (36.7)	<59 years	31 (34.4)
≥59 years	69 (63.3)	≥59 years	59 (65.6)
Histological grade		**Histological grade**	
Well/Moderate	52 (47.7)	Well/Moderate	34 (37.8)
Poor/Undifferentiated	57 (52.3)	Poor/Undifferentiated	56 (62.2)
Tumor size, cm		**Tumor size, cm**	
<5.5	62 (56.9)	<5.5	52 (57.8)
≥5.5	47 (43.1)	≥5.5	38 (42.2)
Tumor, n		**Tumor, n**	
Solitary	105 (96.3)	Solitary	85 (94.4)
Multiple	4 (3.7)	Multiple	5 (5.6)
Tumor location		**Tumor location**	
Cardia	17 (15.6)	Cardia	12 (13.3)
Body	18 (16.5)	Body	18 (20.0)
Antrum	72 (66.1)	Antrum	54 (60.0)
Whole	2 (1.8)	Whole	6 (6.7)
pT status		**pT status**	
T1/T2	33 (30.3)	T1/T2	13 (14.4)
T3/T4	76 (69.7)	T3/T4	77 (85.6)
pN status		**pN status**	
Absent (N0)	27 (24.8)	Absent (N0)	22 (24.4)
Present (N1-3)	82 (75.2)	Present (N1-3)	68 (75.6)
pM status		**pM status**	
M0	95 (87.2)	M0	80 (88.9)

M1	14 (12.8)	M1	10 (11.1)
AJCC stage		**AJCC stage**	
I/II	36 (33.0)	I/II	36 (40.0)
III/IV	73 (67.0)	III/IV	54 (60.0)

Table S2. The relationship between miR-647 expression detected by qPCR and clinicopathologic parameters in 109 primary gastric cancer

Variable	Number	Median expression	*p* Value
Gender			0.8189
Male	70	0.5537±0.04686	
Female	39	0.5373±0.04612	
Median age			0.4478
<59 years	40	0.5821±0.05318	
≥59 years	69	0.5279±0.04447	
Histological grade			0.7275
Well/Moderate	52	0.5353±0.03889	
Poor/Undifferentiated	57	0.5593±0.05523	
Tumor size,cm			0.0319
<5.5	62	0.4842±0.02964	
≥5.5	47	0.6318±0.06752	
Tumor location			0.3958
Cardia/Body	35	0.5054±0.04322	
Antrum/Whole	74	0.5679±0.04604	
pT status			0.0062
T1/T2	33	0.6884±0.08071	
T3/T4	76	0.4868±0.03231	
pN status			0.0046
Absent (N0)	27	0.7149±0.08043	
Present (N1-3)	82	0.4928±0.03518	
AJCC stage			0.0020
I/II	36	0.6962±0.08095	
III/IV	73	0.4746±0.02868	

Table S3. Predicted targets of miR-647 on mRNA 3' UTR region produced by 5 programs

MicroRNA	Gene	miRanda	miRDB	miRWalk	RNA22	Targetscan	SUM
hsa-miR-647	CPEB2	1	1	1	0	1	4
hsa-miR-647	WASF2	1	1	1	0	1	4
hsa-miR-647	SRF	1	1	1	0	1	4
hsa-miR-647	RAB1A	1	1	1	0	1	4
hsa-miR-647	DAB2	1	1	1	0	1	4
hsa-miR-647	MMP14	1	0	1	0	1	3
hsa-miR-647	MMP16	1	0	1	0	1	3
hsa-miR-647	SEMA4D	1	1	0	0	1	3
hsa-miR-647	CHIT1	1	1	1	0	0	3
hsa-miR-647	ZAK	0	1	1	0	1	3
hsa-miR-647	ELMO2	1	0	1	0	1	3
hsa-miR-647	MYH9	1	0	0	0	1	2
hsa-miR-647	MYO1D	1	0	0	0	1	2
hsa-miR-647	MYO6	1	0	0	0	1	2

hsa-miR-647	MYO10	1	0	0	0	1	2
hsa-miR-647	MYOC	1	0	0	0	1	2
hsa-miR-647	MMP8	1	0	1	0	0	2
hsa-miR-647	MMP19	1	0	1	0	0	2
hsa-miR-647	MAGEB1	0	0	1	0	1	2
hsa-miR-647	MMP24	1	0	0	0	0	1
hsa-miR-647	ROCK1	1	0	0	0	0	1
hsa-miR-647	MMP2	1	0	0	0	0	1
hsa-miR-647	MMP15	1	0	0	0	0	1
hsa-miR-647	ABHD12	0	0	0	0	1	1
hsa-miR-647	WIPI2	0	0	0	0	1	1
hsa-miR-647	MYO7A	0	0	1	0	0	1

http://zmf.umm.uni-heidelberg.de/apps/zmf/mirwalk/micrornapredictedtarget.html

Table S4. Pathway enrichment analysis of miR-647 targets

Pathway database	Description of pathway	p^1
GenMAPP	Peptide GPCRs	0.0001
BioCarta	PDGF signaling pathway	0.0008
BioCarta	EGF signaling pathway	0.001
BioCarta	Growth hormone signaling pathway	0.0011
GenMAPP	GPCRs, class A rhodopsin-like	0.0012
BioCarta	MAP kinase signaling pathway	0.0023
BioCarta	Ion channel and phorbal esters signaling pathway	0.0026
GenMAPP	GPCRs, class B secretin like	0.0027
BioCarta	Pertussis toxin-insensitive CCR5 signaling in macrophage	0.0028
BioCarta	Beta-oxidation of fatty acids	0.0038
BioCarta	Thrombin signaling and protease-activated receptors	0.0043
BioCarta	The reactions that feed amino groups into the urea cycle	0.0052
BioCarta	TPO signaling pathway	0.0062
GenMAPP	Calcium channels	0.0104
BioCarta	SODD/TNFR1 signaling pathway	0.0106
BioCarta	How progesterone initiates the oocyte maturation	0.0114
BioCarta	Role of Ran in mitotic spindle regulation	0.0128
BioCarta	Induction of apoptosis through DR3 and DR4/5 death receptors	0.0134
BioCarta	Rho cell motility signaling pathway	0.0134
GenMAPP	Glycolysis and gluconeogenesis	0.016
BioCarta	How does Salmonella hijack a cell	0.0175
BioCarta	CBL mediated ligand-induced downregulation of EGF receptors	0.0201
BioCarta	Segmentation clock	0.0201
BioCarta	Bioactive peptide induced signaling pathway	0.0221
BioCarta	p38 MAPK signaling pathway	0.0221
BioCarta	IL-3 signaling pathway	0.0228
BioCarta	IL-7 signal transduction	0.0256
BioCarta	METS affect on macrophage differentiation	0.0256
BioCarta	PKC-catalyzed phosphorylation of inhibitory phosphoprotein of myosin	0.0256
BioCarta	Role of PI3K subunit p85 in regulation of actin organization and cell migration	0.0256
BioCarta	T cell receptor signaling pathway	0.028
BioCarta	Cadmium induces DNA synthesis and proliferation in macrophages	0.0286
BioCarta	Y branching of actin filaments	0.0286
KEGG	Fatty acid biosynthesis (path 2)	0.0296
BioCarta	Hop pathway in cardiac development	0.0324
BioCarta	Keratinocyte differentiation	0.0328

BioCarta	EPO signaling pathway	0.0348
BioCarta	Role of EGF receptor transactivation by GPCRs in cardiac hypertrophy	0.0348
BioCarta	Role of MAL in Rho-mediated activation of SRF	0.0348
GenMAPP	Ribosomal proteins	0.0358
BioCarta	IGF-1 signaling pathway	0.038
BioCarta	Oxidative stress induced gene expression via Nrf2	0.038
BioCarta	IL-6 signaling pathway	0.0414
BioCarta	Insulin signaling pathway	0.0414
BioCarta	Skeletal muscle hypertrophy is regulated via AKT/mTOR pathway	0.0414
BioCarta	Ceramide signaling pathway	0.0448
BioCarta	IL-2 signaling pathway	0.0448
BioCarta	Inhibition of cellular proliferation by gleevec	0.0448
BioCarta	Nitrogen-depedent regulation of Rtg1 and Rtg3 in TOR pathway	0.0478
BioCarta	CCR3 signaling in eosinophils	0.0482

[1] Based on Fisher's exact test using a 2x2 contingency table

Table S5. Correlation between expression of miR-647 detected by ISH and clinicopathological features of GC patients in cohort 1

	miR-647 expression		
Variable	Low(%)	High(%)	p Value[a]
Gender			0.604
Male	50 (65.8)	20 (60.6)	
Female	26 (34.2)	13 (39.4)	
Median age			0.700
<59 years	27 (35.5)	13 (39.4)	
⩾59 years	49 (64.5)	20 (60.6)	
Histological grade			0.028
Well/Moderate	31 (40.8)	21 (63.6)	
Poor/Undifferentiated	45 (59.2)	12 (36.4)	
Tumor size, cm			0.112
<5.5	47 (61.8)	15 (45.5)	
⩾5.5	29 (38.2)	18 (54.5)	
Tumor location			0.857
Cardia/Body	24 (31.6)	11 (33.3)	
Antrum/Whole	52 (68.4)	22 (66.7)	
pT status			0.001
T1/T2	11 (14.5)	14 (42.4)	
T3/T4	65 (85.5)	19 (57.6)	
pN status			0.000
Absent (N0)	4 (5.3)	23 (69.7)	
Present (N1-3)	72 (94.7)	10 (30.3)	
pM status			0.088
M0	63 (82.9)	32 (97.0)	
M1	13 (17.1)	1 (3.0)	
AJCC stage			0.024
I/II	20 (26.3)	16 (48.5)	
III/IV	56 (73.7)	17 (51.5)	

All data are the number of patients (%).

[a] p values were calculated in SPSS using a chi-square test. p values < .05 were considered to indicate statistical significance. AJCC,

American Joint Committee on Cancer.

Table S6. Correlation between expression of SRF or MYH9 and clinicopathological features of GC patients in cohort 1

Variable	SRF expression			MYH9 expression		
	Low(%)	High(%)	*p* Value[a]	Low(%)	High(%)	*p* Value[a]
Gender			0.691			0.803
Male	26 (66.7)	44 (62.9)		25 (65.8)	45 (63.4)	
Female	13 (33.3)	26 (37.1)		13 (34.2)	26 (36.6)	
Median age			0.897			0.982
<59 years	14 (35.9)	26 (37.1)		14 (36.8)	26 (36.6)	
≥59 years	25 (64.1)	44 (62.9)		24 (63.2)	45 (63.4)	
Histological grade			0.031			0.451
Well/Moderate	24 (61.5)	28 (40.0)		20 (52.6)	32 (45.1)	
Poor/Undifferentiated	15 (38.5)	42 (60.0)		18 (47.4)	39 (54.9)	
Tumor size, cm			0.378			0.142
<5.5	20 (51.3)	42 (60.0)		18 (47.4)	44 (62.0)	
≥5.5	19 (48.7)	28 (40.0)		20 (52.6)	27 (38.0)	
Tumor location			0.280			0.731
Cardia/Body	10 (25.6)	25 (35.7)		13 (34.2)	22 (31.0)	
Antrum/Whole	29 (74.4)	45 (64.3)		25 (65.8)	49 (69.0)	
pT status			0.016			0.116
T1/T2	14 (35.9)	11 (15.7)		12 (31.6)	13 (18.3)	
T3/T4	25 (64.1)	59 (84.3)		26 (68.4)	58 (81.7)	
pN status			0.000			0.000
Absent (N0)	22 (56.4)	5 (7.1)		18 (47.4)	9 (12.7)	
Present (N1-3)	17 (43.6)	65 (92.9)		20 (52.6)	62 (87.3)	
pM status			0.017			0.042
M0	38 (97.4)	57 (81.4)		37 (97.4)	58 (81.7)	
M1	1 (2.6)	13 (18.6)		1 (2.6)	13 (18.3)	
AJCC stage			0.009			0.057
I/ II	19 (48.7)	17 (24.3)		17 (44.7)	19 (26.8)	
III/IV	20 (51.3)	53 (75.7)		21 (55.3)	52 (73.2)	

All data are the number of patients (%).

[a]*p* values were calculated in SPSS using a chi-square test. *p* values < .05 were considered to indicate statistical significance. AJCC, American Joint Committee on Cancer.

Table S7. Correlation between expression of SRF or MYH9 and clinicopathological features of GC patients in cohort 2

Variable	SRF expression			MYH9 expression		
	Low(%)	High(%)	*p* Value[a]	Low(%)	High(%)	*p* Value[a]
Gender			0.436			0.523
Male	23 (71.9)	37 (63.8)		18 (62.1)	42 (68.9)	
Female	9 (28.1)	21 (36.2)		11 (37.9)	19 (31.1)	
Median age			0.161			0.345
<59 years	8 (25.0)	23 (39.7)		8 (27.6)	23 (37.7)	
≥59 years	24 (75.0)	35 (60.3)		21 (72.4)	38 (62.3)	
Histological grade			0.186			0.060
Well/Moderate	15 (46.9)	19 (32.8)		15 (51.7)	19 (31.1)	
Poor/Undifferentiated	17 (53.1)	39 (67.2)		14 (48.3)	42 (68.9)	

Characteristic			p^a			p^a
Tumor size, cm			0.500			0.305
<5.5	20 (62.5)	32 (55.2)		19 (65.5)	33 (54.1)	
≥5.5	12 (37.5)	26 (44.8)		10 (34.5)	28 (45.9)	
Tumor location			0.876			0.038
Cardia/Body	11 (34.4)	19 (32.8)		14 (48.3)	16 (26.2)	
Antrum/Whole	21 (65.6)	39 (67.2)		15 (51.7)	45 (73.8)	
pT status			0.582			0.842
T1/T2	6 (18.8)	7 (12.1)		5 (17.2)	8 (13.1)	
T3/T4	26 (81.2)	51 (87.9)		24 (82.8)	53 (86.9)	
pN status			0.032			0.040
Absent (N0)	12 (37.5)	10 (17.2)		11 (37.9)	11 (18.0)	
Present (N1-3)	20 (62.5)	48 (82.8)		18 (62.1)	50 (82.0)	
pM status			0.969			0.051
M0	29 (90.6)	51 (87.9)		29 (100.0)	51 (83.6)	
M1	3 (9.4)	7 (12.1)		0 (0.0)	10 (16.4)	
AJCC stage			0.059			0.043
I/II	17 (53.1)	19 (32.8)		16 (55.2)	20 (32.8)	
III/IV	15 (46.9)	39 (67.2)		13 (44.8)	41 (67.2)	

All data are the number of patients (%).

[a]*p* values were calculated in SPSS using a chi-square test. *p* values < .05 were considered to indicate statistical significance. AJCC, American Joint Committee on Cancer.

Table S8. Information on antibodies and reagents used for the correlation analysis

Antibody	WB	IHC	IF	IP	Specificity	Source
					mouse	Santa Cruz
anti-GAPDH (sc-365062):	1:1000					
anti-SRF, clone 1E1 (MAB4369)	1:1000	1:100	1:50		mouse	Millipore
anti-SRF(sc-335)				1:50	rabbit	Santa Cruz
Anti-MRTFA (ab115319)				1:50	rabbit	Abcam
anti-MYH9 (sc-98978)	1:1000	1:100	1:50		rabbit	Santa Cruz
anti-Mouse IgG H&L (HRP) (Ab136815)					Goat	Abcam
anti-Rabbit IgG H&L (HRP) (Ab136817)					Goat	Abcam
4', 6-diamidino-2-phenylindole, dihydrochloride (DAPI)(#4083)			0.5µg/ml			Cell Signaling Technology
anti-Rabbit IgG (H+L), F(ab')2 Fragment (Alexa Fluor® 555 Conjugate) (red) (#4413)			1:50		Goat	Cell Signaling Technology
anti-Mouse IgG (H+L), F(ab')2 Fragment (Alexa Fluor® 488 Conjugate) (green) (#4412)			1:50		Goat	Cell Signaling Technology

Table S9. Sequence information used in this study

siRNA	Sequence	
miR-647 mimics	5′ -GUGGCUGCACUCACUUCCUUC-3′	(sense)
	5′ -AGGAAGUGAGUGCAGCCACUU-3′	(antisense)
Negative control	5′ -UUCUCCGAACGUGUCACGUTT-3′	(sense)
	5′ -ACGUGACACGUUCGGAGAATT-3′	(antisense)
miR-647 inhibitor	5′ -GAAGGAAGUGAGUGCAGCCAC-3′	
Inhibitor negative control	5′ -CAGUACUUUUGUGUAGUACAA-3′	

hsa-miR-647 probe	5'-GAAGGAAGTGAGTGCAGCCAC-3'	
U6 probe	5'-CACGAATTTGCGTGTCATCCTT-3'	
Scramble-miR probe	5'-GTGTAACACGTCTATACGCCCA-3'	
SRF siRNA1	5'-CCACAACAGACCAGAGAAUTT-3'	
SRF siRNA2	5'-CCCUGUUUCAGCAGUUCAGTT-3'	
SRF siRNA3	5'-GU UCCUGACAG CAUCAUCUTT-3'	

Table S10. Information on qPCR primers used for this study

Gene	Primer sequence		GC(%)	Tm(°C)
MYH9	Forward	5'-ACCATGGAGGCCATGAGGATTA-3';	50	64.8
	Reverse	5'-CGATGTTGCCGAGCTGAAGA-3';	55	64.9
SRF	Forward	5'-AGAATGAGTGCCACTGGCTTTG-3';	50	63.8
	Reverse	5'-CTGCTGACTTGCATGGTGGTAG-3';	54.5	63.1
ROCK1	Forward	5'-AGGAAGGCGGACATATTAGTCCCT-3';	50	72
	Reverse	5'-AGACGATAGTTGGGTCCCGGC-3';	61.9	68
ELMO2	Forward	5'-CGTTGCCAAACCCAGAGTAT-3';	50	60
	Reverse	5'-TGGAGGTGTGAGATGAGCTG-3';	55	62
ZAK	Forward	5'-TCAGACTCCACCTTTGTTTGCA-3';	45.5	64
	Reverse	5'-GTAGGTGCTTGGAACTCTAGTTTTGA-3';	42.3	74
GAPDH	Forward	5'-GCACCGTCAAGGCTGAGAAC-3';	60	63.3
	Reverse	5'-TGGTGAAGACGCCAGTGGA-3';	57.9	64

Table S11. Information on plasmids used in this study.

Plasmid	sequencing primers	plasmid vector	Cloning sites
SRF	Forward: 5'-TTCAGCAAGAGGAAGACGG-3'; Reverse: 5'-AACGCACACCGGCCTTATTC-3'.	GV311	Xho I/BamH I
MYH9	Forward: 5'-GCGGTAGGCGTGTACGGT-3'; Reverse: 5'-CGGACACGCTGAACTTGT-3'	EX-T1335-M98-5	
SRF-3'UTR-WT1 (WT1)	Forward: 5'-AGGAACGGGCAGCCACAGGA-3'; Reverse: 5'-GCGAGGTCCGAAGACTCATTT-3'	GV306	Xbal/Xbal
SRF-3'UTR-Mut1 (Mut1)	Forward: 5'-GTTGCCTTTTCACGTTTTC-3'; Reverse: 5'-GCGAGGTCCGAAGACTCATTT-3'	GV306	Xbal/Xbal
SRF-3'UTR-Mut2 (Mut2)	Forward: 5'-GTTGCCTTTTCACGTTTTC-3'; Reverse: 5'-GCGAGGTCCGAAGACTCATTT-3'	GV306	Xbal/Xbal
SRF-3'UTR-WT2 (WT2)	Forward: 5'-AGGAACGGGCAGCCACAGGA-3'; Reverse: 5'-GCGAGGTCCGAAGACTCATTT-3'	GV306	Xbal/Xbal
SRF-3'UTR-Mut3 (Mut3)	Forward: 5'-AGGAACGGGCAGCCACAGGA-3'; Reverse: 5'-GCGAGGTCCGAAGACTCATTT-3'	GV306	Xbal/Xbal
MYH9-3'UTR-WT (WT3)	Forward: 5'-GGCTTCTCCCAACACTCT-3'; Reverse: 5'-GCGAGGTCCGAAGACTCATTT-3'	GV306	Xbal/Xbal
MYH9-3'UTR-Mut (Mut4)	Forward: 5'-GGCTTCTCCCAACACTCT-3'; Reverse: 5'-GCGAGGTCCGAAGACTCATTT-3'	GV306	Xbal/Xbal
UpMYH9-1	Forward: 5'-CTAGCAAAATAGGCTGTCCC-3'; Reverse: 5'-CTTTATGTTTTTGGCGTCTTCCA-3'	pGL3-Basic	KpnI/HindIII
UpMYH9-2	Forward: 5'-CTAGCAAAATAGGCTGTCCC-3'; Reverse: 5'-CTTTATGTTTTTGGCGTCTTCCA-3'	pGL3-Basic	KpnI/HindIII
UpMYH9-3	Forward: 5'-CTAGCAAAATAGGCTGTCCC-3'; Reverse: 5'-CTTTATGTTTTTGGCGTCTTCCA-3'	pGL3-Basic	KpnI/HindIII
UpMYH9-4	Forward: 5'-CTAGCAAAATAGGCTGTCCC-3'; Reverse: 5'-CTTTATGTTTTTGGCGTCTTCCA-3'	pGL3-Basic	KpnI/HindIII
UpMYH9-5	Forward: 5'-CTAGCAAAATAGGCTGTCCC-3';	pGL3-Basic	KpnI/HindIII

	Reverse: 5'-CTTTATGTTTTTGGCGTCTTCCA-3'			
UpMYH9-6	Forward: 5'-CTAGCAAAATAGGCTGTCCC-3';	pGL3-Basic	KpnI/HindIII	
	Reverse: 5'-CTTTATGTTTTTGGCGTCTTCCA-3'			
SRF ShRNA2#	Reverse:5'-AAGCTGCAATAAACAAGTTCCTCT-3';	LV3	BamHI/EcoRI	

Supplementary Materials and Methods

Reagents, Lentiviral Transduction, Oligonucleotide and Plasmid Transfections

CCG-1423 ($C_{18}H_{13}ClF_6N_2O_3$), [N-[2-(4-chloroanilino)-1-methyl-2-oxoethoxy]-3,5-bis(trifluoromethyl)benzamide] were bought from MedChemExpress. Agomir-647 (microN™ hsa-miR-647 agomir, miR40003317-1-10) and agomir-NC were commercially synthesized by RiboBio (Guangzhou, China).

The full length of the has-miR-647 precursor (pre-miR-647) was chemically synthesized by GeneChem and introduced into the GV217 lentiviral vector (GeneChem, Shanghai, China) in the unique EcoRI site, which was confirmed by using nucleotide sequencing. This constructed vector was transfected into lentiviral packaging cell lines HEK293T, and lentiviral particles encoding miR-647 (LV-miR-647) were collected from the supernatant of the transfected cells. MGC 80-3 and AGS cells (1×10^5) were infected with 1×10^7 lentivirus transducing in the presence of 10 mg/ml polybrene. Three days after infection, the efficiency of infection was evaluated by observing the EGFP expression in a fluorescence microscope (IX71, Olympus, Tokyo, Japan). The overexpression of miR-647 in cells were confirmed by qPCR analysis.

MiR-647 mimics, inhibitors and human SRF siRNAs (siRNA#1-3) were synthesized by GenePharma (Suzhou, China). To construct human SRF expression plasmid, the 1574bp DNA fragment of human SRF was subcloned into the GV311 plasmid vector (GeneChem, Shanghai, China) using the Xho I and BamH I sites. The GV311 vector contains a monomeric (m)Cherry coding sequence and a neomycin resistance cassette (Table S11). Human MYH9 expression plasmid (EX-T1335-M98-5) was constructed by GeneCopoeia, which contains an eGFP coding sequence and a neomycin resistance cassette. Since siRNA#2 was confirmed to be more effective (Figure S4), its corresponding short-hairpin RNA (shRNA#2) was subcloned into LV3 plasmid vector (GenePharma, Suzhou, China), which contains a GFP coding sequence and a puromycin resistance cassette. To construct plasmids used in dual-luciferase reporter assays for detecting the binding of miR-647 to SRF or MYH9 3'UTR, two wild-type SRF 3'UTR fragments (containing three miR-647 binding sites) and three mutant fragments (mutant in miR-647 binding sites) were chemically synthesized and cloned into the GV306 luciferase reporter vector at an unique XbaI site, which is downstream of the Firefly luciferase stop codon and is followed by the Renilla luciferase gene. To construct plasmids used in dual-luciferase reporter assays for detecting the binding of SRF to MYH9 promoter, six DNA fragments with different lengths were cloned from the predicted human MYH9 promoter and inserted into the pGL3 vector (Promega, Madison, WI, USA) using the KpnI/HindIII sites. For transfections, cells were seeded into plates overnight, and experiments were performed with Lipofectamine 3000 reagent (Life Technologies, USA) according to the manufacturer's instructions. To establish stable cell lines, puromycin or G418 was added to cells according to the manufacturer's instructions. The miRNA mimics, inhibitors, siRNAs and plasmids were showed in table S9 and S11.

RNA Isolation, Quantitative Real-time PCR (qPCR) and Western Blot

Total RNA from tissue samples and cultured cells was extracted using TRIzol reagent (Invitrogen). Quantitative real-time PCR (qPCR) assays were carried out to detect mRNA expression using the PrimeScript RT Reagent Kit (TaKaRa) and SYBR Premix Ex Taq (TaKaRa) according to the manufacturer's instructions. GAPDH was used as an internal control. The primers are listed in Table S10. For miRNA expression analysis, reverse transcription was performed using a ReverTra Ace qPCR RT Kit (Toyobo) with a miR-647 bulge-loop RT primer. The bulge-loop RT primer and qPCR primers specific for miR-647 were designed and synthesized by RiboBio (RiboBio). The U6 small nuclear RNA was used as an internal control. Data analysis was performed using the $2^{-\Delta\Delta Ct}$ method [3].

According to standard Western blot procedures, briefly, proteins were separated by 8% SDS-PAGE and then transferred to nitrocellulose membrane (Bio-Rad). After blocking in 5% nonfat milk, the membranes were incubated with special primary antibodies (Table S8). The proteins were visualized with Immobilon ECL (Millipore).

Pathway Enrichment Analysis, Expression Data Analysis in Gene Expression Omnibus (GEO) Database and The Cancer Genome Atlas (TCGA)

As described previously [4], pathway enrichment analysis was performed using the miRGator [5] online software (Nam, et al., Nucleic Acids Research. 36: D159-64; http://genome.ewha.ac.kr/miRGator) on the gene targets of miR-647 predicted in the miRBase Targets database (http://microrna.sanger.ac.uk/targets). Cell motility-associated signal pathways were listed in Figure 2A.

All expression profiling data of miRNA and mRNA analyzed in this study were downloaded from the Gene Expression Omnibus (GEO, http://www.ncbi.nlm.nih.gov/geo/) (GSE36968 [6], GSE63288 [7] and GSE84784 (https://www.ncbi.nlm.nih.gov/geo/query/acc.cgi?acc=GSE84784)) and The Cancer Genome Atlas (TCGA, http://cancergenome.nih.gov/).

Monolayer Wound Healing Assay

MGC 80-3 cells were transfected with LV-NC, LV-miR-647, LV-miR-647/miR-647 inhibitors and LV-miR-647/miR-647 inhibitor negative control. The expression change of miR-647 was confirmed by qPCR. Before seeding the cells, five parallel lines were drawn on the underside of each well with a marker pen. Approximately $5×10^5$ cells per well were seeded into 6-well plates. After cells had become adherent, five parallel scratches or 'wounds' (wide approximately equal to 500 µm) were made perpendicular to the marked lines using a yellow pipette tip (200µl). The migration of cells into the 'wounds' was observed using an inverted microscope (IX71, Olympus, Tokyo, Japan), and images of areas flanking the intersections of the 'wound' and the marked lines were taken at regular intervals over the course of 24h.

Cell 3D Migration and Invasion Assays

For migration assays, transfected cells were harvested and resuspended in serum-free RPMI-1640 medium, and $5×10^4$ cells were placed into 6.5-mm Boyden chambers with 8-µm pores (Corning Costar, Corning, NY, USA). For invasion assays, $1×10^5$ cells were placed into chambers coated with Matrigel (BD Biosciences, Boston, MA, USA). The chambers were then inserted into the wells of a 24-well plate and incubated for 24 h in RPMI-1640 medium with 10% fetal bovine serum prior to examination. The cells remaining on the upper surface of the membrane were removed, and the cells adhering to the lower surface were fixed, stained in a dye solution containing 0.05% crystal violet, and counted under a microscope (IX71, Olympus, Tokyo, Japan) to determine their relative numbers. For each experiment, the number of cells in at least five random field on the underside of the filter t was counted, and three independent filters were analyzed.

Luciferase Reporter Assay

Approximately $1×10^5$ cells per well were seeded into 6-well plates for luciferase reporter assays. To identify the miR-647 binding sites in 3'UTR of SRF and MYH9 mRNAs, MGC 80-3 and AGS stably expressing miR-647 were transfected with the appropriate plasmids (WT1-2 and Mut 1-4) in 24-well plates. To confirm SRF targeted to the promoter of MYH9, MGC 80-3 was co-transfected with SRF plasmid, Renilla luciferase plasmid and the full-length MYH9 promoter construct or truncation constructs. Cells were harvested and lysed for luciferase assays 24h after transfection. Luciferase assays were performed using a Dual-Luciferase Reporter Assay System (Promega, Madison, WI, USA) in a Modulus™ II Microplate Multimode Reader (Promega) according to the manufacturer's protocols. Firefly luciferase (FLuc) activity was measured and normalized against the Renilla luciferase (RLuc) activity. All the experiments were carried out in triplicate.

Chromatin Immunoprecipitation (ChIP) Assay

The ChIP assay was performed on MGC 80-3 and AGS cells using the Pierce™ Agarose ChIP kit (Pierce; Thermo Scientific, Rockford, IL, USA) according to the manufacturer's protocol. Immunoprecipitation was carried out using rabbit polyclonal SRF antibody (sc-335). An unrelated rabbit IgG was used as a negative control. To amplify the potential SRF-binding site from nucleotides -490 to -481 in the promoter of MYH9, qPCR was performed using the forward primer 5'-AAAGAGGCAGGGTCAGGAAT-3' and the reverse primer 5'-ATCCCACCACAAGGACAGAT-3'. The anti-RNA polymerase II (anti-RNAPII) antibody and GAPDH qPCR primers were provided as a positive control in the kit for assay technique and reagent integrity. Data analysis was performed using the $2^{(-\Delta\Delta Ct\ [ChIP/NIS])}$ method [8].

In Vivo Metastasis Assay

Five- to 6-week-old male athymic BALB/c nu/nu mice were purchased from the Central Laboratory of Animal Science at Southern Medical University (Guangzhou, China). The mice were maintained at the Laboratory Animal Centre of Nanfang hospital in a specific pathogen-free environment. For in vivo metastasis assays, $5×10^6$ MGC 80-3 cells infected with either the miR-647-overexpressing lentivirus or the mock lentivirus were injected subcutaneously into the right flank of nude mice (n=3 per group). Tumors were measured with calipers every 3 days after injection, and the tumor volumes were calculated according to the following formula: 0.5 × length × $width^2$. Tumors were selected for orthotopic implantation at an average size of $0.5\ cm^3$ and tissue was cut into $2×2×2\ mm^3$ pieces. Superficial regions of the tumors were used for implantation and all sampled tumors were examined histologically to confirm that areas of the tumor corresponding to the sampled regions contained viable tissue. Implantation was performed according to the previous studies [9, 10] with some modifications. In brief, the mice were randomly assigned and fasted overnight. The stomach was exteriorised through a small midline laparotomy and a piece of tumor tissue sutured to the greater curvature side of the gastric antrum surface with a single Maxon 7/0 suture, leaving the tumor tissue buried in a 'pouch' consisting of a double caecal wall on each side. After implantation, the abdominal wall was closed in two layers with Dexon 5/0. Six weeks later, the mice were killed and all organs were removed for examination. Hepatic, intestinal and peritoneal metastases were detected by HE and IHC staining and quantified by counting metastatic lesions in each section. All in vivo experiments above were performed according to our institution's guidelines for the use of laboratory animals and were approved by the Institutional Animal Care and Use Committee of Nanfang Hospital.

Therapeutic experiments. For in vivo treatment assays, we constructed metastatic models of human gastric cancer using orthotopic implantation as described above. For CCG-1423 treatment assays, two weeks after orthotopic implantation, mice were administrated by intraperitoneal injection of CCG-1423 (0.15 mg/kg/d)[11] or vehicle alone (DMSO) for 2 weeks, and repeated it again 6 weeks after orthotopic implantation. For agomir-647 and CCG-1423 combination treatment assays, two weeks after orthotopic implantation, mice were administrated intravenously by tail vein injection of agomir-647 (80mg/kg/3d) [12] or agomir negative control (NC) for 5 times and by intraperitoneal injection of CCG-1423 (0.15 mg/kg/d) or vehicle alone (DMSO) for 2 weeks. Six weeks after orthotopic implantation, repeated the combination treatment again, as showed in Figure S7. Eight weeks after orthotopic implantation, the mice were killed and all organs were removed for examination. Primary tumors and metastatic nodules were detected by HE and IHC staining. All in vivo treatment assays above were performed according to our institution's guidelines for the use of laboratory

animals and were approved by the Institutional Animal Care and Use Committee of Nanfang Hospital.

Hematoxylin-eosin (HE) Staining, Immunohistochemical (IHC) Staining and Immunofluorescence (IF) Staining

Complete sectioning was performed for all the human GC tissues, orthotopic implantation tumors and metastases to ensure a precise diagnosis. 4 μm-thick formalin-fixed and paraffin embedded sections were prepared for HE staining. Briefly, paraffin embedded sections were deparaffinized and rehydrated in a series of xylene and ethanol baths of decreasing concentration. Slides were put in hematoxylin solution for 1 min, followed by 1% alcoholic hydrochloric acid for 3 seconds, and then eosin solution for 1 min. Immunohistochemistry staining (IHC) was performed using a Dako Envision System (Dako, Carpinteria, CA) following the manufacturer's recommended protocol. For incubation with primary mAb, tissue slides were incubated at 4°C overnight with mouse anti-SRF mAb (1:100; Millipore) and rabbit anti-MYH9 mAb (1:100; Santa Cruz). Negative controls were treated identically, but without the primary antibody. Scoring was measured as described before [13]: scored 0, absent cell cytoplasm staining; scored 1, weak cell cytoplasm staining; scored 2, moderate cell cytoplasm staining; scored 3, strong cell cytoplasm staining. Immunofluorescence staining for SRF and MYH9 was performed on GC cells and frozen sections of humanGC tissues using mouse anti-SRF mAb (1:50; Millipore) and rabbit anti-MYH9 mAb (1:50; Santa Cruz). Cells were plated onto coverslips, washed with phosphate-buffered saline, fixed in 4% paraformaldehyde for 10 minutes, permeabilized with 0.25% Triton for 5 minutes and incubated with primary antibodies at 4°C overnight, followed by a 1-hour incubation with fluorescently conjugated secondary antibodies. Nuclei were counterstained with 4',6-diamidino-2-phenylindole (DAPI; CST), and then the coverslips were imaged via a confocal laser scanning microscope (FV1000; Olympus, Center Valley, PA). The primary antibodies and DAPI are listed in Table S8.

References

1. Morita T, Mayanagi T, Sobue K. Dual roles of myocardin-related transcription factors in epithelial-mesenchymal transition via slug induction and actin remodeling. Journal of Cell Biology. 2007; 179: 1027-42.

2. Medjkane S, Perez-Sanchez C, Gaggioli C, Sahai E, Treisman R. Myocardin-related transcription factors and SRF are required for cytoskeletal dynamics and experimental metastasis. Nat Cell Biol. 2009; 11: 257-68.

3. Meng X, Wu J, Pan C, Wang H, Ying X, Zhou Y, et al. Genetic and epigenetic down-regulation of microRNA-212 promotes colorectal tumor metastasis via dysregulation of MnSOD. Gastroenterology. 2013; 145: 426-36 e1-6.

4. Patnaik SK, Kannisto E, Knudsen S, Yendamuri S. Evaluation of microRNA expression profiles that may predict recurrence of localized stage I non-small cell lung cancer after surgical resection. Cancer Res. 2010; 70: 36-45.

5. Nam S, Kim B, Shin S, Lee S. miRGator: an integrated system for functional annotation of microRNAs. Nucleic Acids Research. 2008; 36: D159-D64.

6. Kim YH, Liang H, Liu XP, Lee JS, Cho JY, Cheong JH, et al. AMPK alpha Modulation in Cancer Progression: Multilayer Integrative Analysis of the Whole Transcriptome in Asian Gastric Cancer. Cancer Research. 2012; 72: 2512-21.

7. Chang HR, Nam S, Kook MC, Kim KT, Liu X, Yao H, et al. HNF4alpha is a therapeutic target that links AMPK to WNT signalling in early-stage gastric cancer. Gut. 2016; 65: 19-32.

8. Dong P, Karaayvaz M, Jia N, Kaneuchi M, Hamada J, Watari H, et al. Mutant p53 gain-of-function induces epithelial-mesenchymal transition through modulation of the miR-130b-ZEB1 axis. Oncogene. 2013; 32: 3286-95.

9. Pocard M, Tsukui H, Salmon RJ, Dutrillaux B, Poupon MF. Efficiency of orthotopic xenograft models for human colon cancers. In Vivo. 1996; 10: 463-9.

10. Furukawa T, Fu X, Kubota T, Watanabe M, Kitajima M, Hoffman RM. Nude mouse metastatic models of human stomach cancer constructed using orthotopic implantation of histologically intact tissue. Cancer Res. 1993; 53: 1204-8.

11. Jin WZ, Goldfine AB, Boes T, Henry RR, Ciaraldi TP, Kim EY, et al. Increased SRF transcriptional activity in human and mouse skeletal muscle is a signature of insulin resistance. Journal of Clinical Investigation. 2011; 121: 918-29.

12. Zhang LF, Lou JT, Lu MH, Gao CF, Zhao S, Li BA, et al. Suppression of miR-199a maturation by HuR is crucial for hypoxia-induced glycolytic switch in hepatocellular carcinoma. Embo Journal. 2015; 34: 2671-85.

13. Zheng B, Liang L, Wang C, Huang S, Cao X, Zha R, et al. MicroRNA-148a suppresses tumor cell invasion and metastasis by downregulating ROCK1 in gastric cancer. Clin Cancer Res. 2011; 17: 7574-83.